Inverse finite element modelling of shells using the degenerated-solid approach

Víctor D. Fachinotti[a], Alejandro E. Albanesi[a], José M. Martinez Valle[b]

[a] *Centro de Investigación de Métodos Computacionales(CIMEC), Universidad Nacional del Litoral (UNL)/ Consejo Nacional de Investigaciones Científicas y Técnicas (CONICET), Predio CCT-CONICET Santa Fe, Colectora Ruta Nac. 168, Paraje El Pozo, 3000, Santa Fe, Argentina*

[b] *Departamento de Mecánica, Escuela Politécnica Superior, Universidad de Córdoba, Edificio Leonardo da Vinci, Campus de Rabanales, 14071, Córdoba, España*

Abstract

The inverse finite element method (IFEM) for degenerated-solid shells is introduced. IFEM allows to determine the undeformed shape of a body (in this case, a shell-like body) such that it attains a desired shape after large elastic deformations. The model is based on the degenerated-solid approach, which enables the use of the standard constitutive laws of Solid Mechanics. A benchmark for validation purposes is first passed. Then, the skills of IFEM for inverse design are demonstrated by means of an application to the design of a micro-valve.

Keywords: Inverse Finite Element Method; degenerated-solid shells; Mixed Interpolation of Tensorial Components; large elastic deformations.

1. Introduction

The Inverse Finite Element Method (IFEM) is intrinsically the FEM applied to the problem of determining the undeformed configuration of a body when the deformed configuration as well as the actuating loads are known.

This kind of problem -also known as Inverse Design problem- often arises in the design of compliant structures or mechanisms suffering large elastic displacements and/or rotations, for instance: a gasket that deforms to the desired shape under given loads [1]; a rubber seal that closes a given channel under a given pressure [2]; a turbine blade that attains an optimal shape at a certain angular speed [3]; an S-clutch whose shoes exactly engage the friction surface of the given drum at a given angular speed [4, 5]; a device that folds an intraocular lens in such a way that facilitates its implantation into the eye [6], among other interesting applications developed in the just-cited works.

Beyond the field of inverse design, Lu and Zhou [7, 8] proposed a singular application of IFEM to the prevention of aneurysms, taking the *in vivo* image of an aneurysm as the known deformed configuration under a known pressure.

All these inverse problems could be solved using systematized "trial-and-error" methods from Optimization Theory, considering any measure of the closeness to the desired deformed configuration as the cost function to be minimized. At each iteration of the optimization problem, a nonlinear (direct) equilibrium equation has to be solved to determine the cost function. On the meanwhile, IFEM solves only one nonlinear equilibrium equation for determining the desired deformed configuration, which is approximately as computationally expensive as only one iteration of an optimization problem. This was illustrated by Albanesi et al. [4, 5], who used IFEM to design a compliant gripper, originally designed by Lan and Cheng [9] by solving an optimization problem.

In our previous works, IFEM was introduced for 3D solids [3] and 3D beams [4, 5]. The current work is a step towards the completion of our

IFEM library by introducing shell elements.

Zhou and Lu [8] introduced IFEM for shells using the stress-resultant approach proposed by Simo et al. [10]. Models based in this approach need specialized constitutive equations for the accross-the-thickness membrane and shear stress resultants and stress couple, as described in the pioneering work of Simo and Fox [11].

In this work, the degenerated-solid approach for shells, originally proposed by Ahmad et al. [12] and extended to nonlinear geometrical analysis by Ramm [13], is preferred. This approach is characterized by defining the stress itself (rather than the stress resultants) using the same constitutive equations as those of Solid Mechanics. This attribute of the degenerated-solid shells has been determinant of our choice. Then, as original contribution, we introduce IFEM in the context of degenerated-solid shells.

The low-order displacement-based shell finite elements predict spurious shear stresses and, as result, exhibit artificially high stiffness. This is the well-known"shear locking" defect [14], which can circumvented by using appropriate mixed finite elements. In this work, recourse is made to the MITC formulation, originally proposed by Dvorkin and Bathe [15] for bi-linear 4-node quadrangles and extended by Bucalem and Bathe [16] for bi-quadratic 9-node and bi-cubic 16-node quadrangles. MITC, which stands for Mixed Interpolation of Tensorial Components, implies that the components of the strain tensor are interpolated independently of the displacements in order to preclude shear locking.

As example of application and validation of the current IFEM for shells, we solve first a popular benchmark problem for linear-elastic shells with large

deflections and rotations [17]. Finally, the ability of IFEM for inverse design is shown by the design of a compliant microvalve to close a given channel when the pressure drop attains a prescribed value, giving a more efficient alternative to that originally proposed to Seidemann et al. [18].

2. Formulation of the degenerated-solid shell finite element

The aim of this Section is to give a brief summary of the formulation of FEM for degenerated-solid shells, that already classical in "direct" FEM. Specifically, we describe the so-called "basic shell" model [19, 20], which is based on the Mindlin-Reissner kinematic hypothesis: those straight fibers that are normal to the midsurface of the shell when it is undeformed remain straight and unstretched during deformation. The "basic shell" model is well-suited for thin to moderately thick shells, offering the best compromise between simplicity and applicability in FEM for shells.

As corollary, we arrive at the system of discrete nonlinear equations governing the equilibrium of geometrically nonlinear degenerated-solid shells in "direct" FEM, taken as starting point for the development of IFEM for degerated-solid shells in the next section.

2.1. Kinematic hypotheses for shells

Let $\mathcal{B}^0$ represent the solid-shell body shown in Figure 1. The geometry of the shell is defined by its midsurface $\mathcal{S}^0$ and the thickness of the shell at each point of the midsurface. Let $\{\xi_1, \xi_2, \xi_3\}$ be a system of natural coordinates, such that ξ_1 and ξ_2 vary through the midsurface $\mathcal{S}^0$ and ξ_3 varies across the thickness of the shell, with $-1 \leq \xi_i \leq 1$ and $\xi_3 = 0$ at the midsurface. Then,

the position of any point $\boldsymbol{X} \in \mathcal{B}^0$ can be expressed as a function of the natural coordinates as follows:

$$\boldsymbol{X}(\xi_1, \xi_2, \xi_3) = \bar{\boldsymbol{X}}(\xi_1, \xi_2) + \xi_3 \frac{H}{2} \boldsymbol{T}(\xi_1, \xi_2), \tag{1}$$

where $\bar{\boldsymbol{X}} \in \mathcal{S}^0$, $\boldsymbol{T}$ is the unit vector known as material director, and $H = H(\xi_1, \xi_2)$ is the thickness of the undeformed shell.

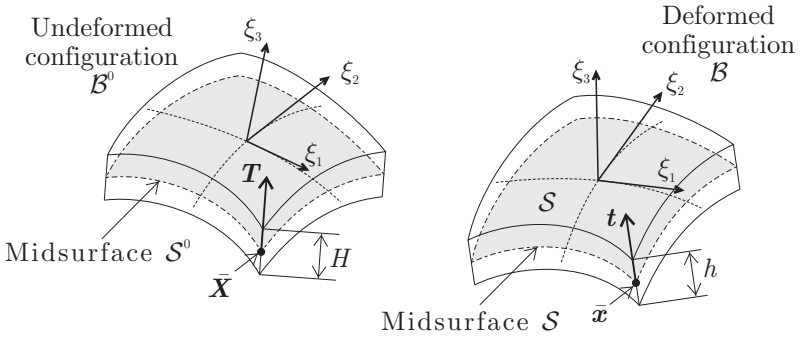

Figure 1: Geometric representation of the undeformed and deformed configurations of a shell.

Let $\mathcal{B}$ be the deformed configuration of the shell, with midsurface $\mathcal{S}$. After deformation, the point $\boldsymbol{X} \in \mathcal{B}^0$ occupies the position $\boldsymbol{x} \in \mathcal{B}$:

$$\boldsymbol{x}(\xi_1, \xi_2, \xi_3) = \bar{\boldsymbol{x}}(\xi_1, \xi_2) + \xi_3 \frac{h}{2} \boldsymbol{t}(\xi_1, \xi_2), \tag{2}$$

where $\bar{\boldsymbol{x}} \in \mathcal{S}$, $\boldsymbol{t}$ is the unit vector known as spatial director, and $h = h(\xi_1, \xi_2)$ is the thickness of the undeformed shell.

In this work, we adopt the "basic shell" model [19, 20] based on the Mindlin-Reissner plate theory, according to which $\boldsymbol{t}$ is not necessarily normal to $\mathcal{S}$ if $\boldsymbol{T}$ is normal to $\mathcal{S}^0$ (and viceversa) as effect of shear deformation. Further, as a consequence of the Mindlin-Reissner assumption, the strain

normal to the midsurface is null [20], so that the thickness of the shell remains constant during deformation, i.e., $h = H$.

Inside a generic finite element with nodes $i = 1, 2, \ldots, N$, the positions $\boldsymbol{x} \in \mathcal{B}$ and $\boldsymbol{X} \in \mathcal{B}^0$ are isoparametrically interpolated from their respective nodal values, as follows:

$$\boldsymbol{X}(\xi_1, \xi_2, \xi_3) = \varphi_i(\xi_1, \xi_2) \left[\bar{\boldsymbol{X}}_i + \frac{\xi_3}{2} h(\xi_1, \xi_2) \boldsymbol{T}_i \right] = \boldsymbol{\Phi}(\xi_1, \xi_2, \xi_3) \boldsymbol{Q}, \tag{3}$$

$$\boldsymbol{x}(\xi_1, \xi_2, \xi_3) = \varphi_i(\xi_1, \xi_2) \left[\bar{\boldsymbol{x}}_i + \frac{\xi_3}{2} h(\xi_1, \xi_2) \boldsymbol{t}_i \right] = \boldsymbol{\Phi}(\xi_1, \xi_2, \xi_3) \boldsymbol{q}, \tag{4}$$

with

$$\boldsymbol{\Phi} = \left[\varphi_1 \boldsymbol{I}_{3\times 3} \quad \tfrac{\xi_3}{2} h \varphi_1 \boldsymbol{I}_{3\times 3} \quad \cdots \quad \varphi_N \boldsymbol{I}_{3\times 3} \quad \tfrac{\xi_3}{2} h \varphi_N \boldsymbol{I}_{3\times 3} \right], \tag{5}$$

$$\boldsymbol{Q} = \begin{bmatrix} \bar{\boldsymbol{X}}_1 \\ \boldsymbol{T}_1 \\ \vdots \\ \bar{\boldsymbol{X}}_N \\ \boldsymbol{T}_N \end{bmatrix}, \qquad \boldsymbol{q} = \begin{bmatrix} \bar{\boldsymbol{x}}_1 \\ \boldsymbol{t}_1 \\ \vdots \\ \bar{\boldsymbol{x}}_N \\ \boldsymbol{t}_N \end{bmatrix}, \tag{6}$$

where $(\bar{\boldsymbol{X}}_i, \boldsymbol{T}_i)$ defines the position of node i in the finite element mesh representing $\mathcal{B}^0$ (known for FEM, unknown for IFEM), $(\bar{\boldsymbol{x}}_i, \boldsymbol{t}_i)$ defines the position of node i in the mesh representing $\mathcal{B}$ (unknown for FEM, known for IFEM), and $\varphi_i = \varphi_i(\xi_1, \xi_2)$ is the 2-D shape function associated to node i; $\boldsymbol{I}_{3\times 3}$ is the 3×3-identity matrix.

The deformation of the shell can be measured using the Green-Lagrange strain tensor, which can be expressed as

$$\boldsymbol{E} = \underbrace{\frac{1}{2} \left(\boldsymbol{g}_\alpha \cdot \boldsymbol{g}_\beta - \boldsymbol{G}_\alpha \cdot \boldsymbol{G}_\beta \right)}_{E^{\text{cov}}_{\alpha\beta}} \boldsymbol{G}^\alpha \otimes \boldsymbol{G}^\beta, \tag{7}$$

where $E^{\text{cov}}_{\alpha\beta}$ are the so-called covariant components of $\boldsymbol{E}$, $\boldsymbol{g}_\alpha = \partial \boldsymbol{x}/\partial \xi_\alpha$ and $\boldsymbol{G}_\alpha = \partial \boldsymbol{X}/\partial \xi_\alpha$ are the spatial and convective basis vectors, respectively, and $\boldsymbol{G}^\alpha$ is a vector of the base reciprocal to $\{\boldsymbol{G}_\alpha\}$, so that $\boldsymbol{G}^\alpha \cdot \boldsymbol{G}_\beta = \delta^\alpha_\beta$.

Using FEM, the covariant strain components $E^{\text{cov}}_{\alpha\beta}$ take the form

$$E^{\text{cov}}_{\alpha\beta} = \frac{1}{2}\left(\boldsymbol{q}^T \boldsymbol{A}_{\alpha\beta} \boldsymbol{q} - \boldsymbol{Q}^T \boldsymbol{A}_{\alpha\beta} \boldsymbol{Q}\right), \tag{8}$$

where $\boldsymbol{A}_{\alpha\beta}$ is the $6N \times 6N$-symmetric matrix defined by

$$\boldsymbol{A}_{\alpha\beta} = \frac{1}{2}\left(\frac{\partial \boldsymbol{\Phi}^T}{\partial \xi_\alpha}\frac{\partial \boldsymbol{\Phi}}{\partial \xi_\beta} + \frac{\partial \boldsymbol{\Phi}^T}{\partial \xi_\beta}\frac{\partial \boldsymbol{\Phi}}{\partial \xi_\alpha}\right). \tag{9}$$

2.2. Cure of shear locking

The stiffness of low-order finite elements increases spuriously as the thickness/in-plane dimension of the element decreases. This is the well-known "shear locking" defect, which affects even cubic-order elements.

One of the simpler cures to "shear locking" is the use of the "assumed-strain" technique. Particularly, we use the technique called MITC (for Mixed Interpolation of Tensorial Components), originally proposed by Dvorkin and Bathe [15].

The MITC technique proposes to replace each covariant strain field $E^{\text{cov}}_{\alpha\beta}$, that defined by equation (8), by an "assumed" field $\tilde{E}^{\text{cov}}_{\alpha\beta}$. Inside each MITC finite element, the assumed field $\tilde{E}^{\text{cov}}_{\alpha\beta}$ is defined such as it coincides with $E^{\text{cov}}_{\alpha\beta}$ at a series of "tying" points:

$$\tilde{E}^{\text{cov}}_{\alpha\beta}(\xi^I_1, \xi^I_2, \xi^I_3) \equiv E^{\text{cov}}_{\alpha\beta}(\xi^I_1, \xi^I_2, \xi^I_3) \qquad I = 1, 2, \ldots, n_{\alpha\beta}, \tag{10}$$

where $(\xi^I_1, \xi^I_2, \xi^I_2)$ are the natural coordinates of the tying point I.

In quadrangular MITCn elements (where n stands for the number of nodes of the element, e.g., MITC4 [15], MITC9, MITC16 [16]), the assumed

strain can be defined as

$$\tilde{E}^{\text{cov}}_{\alpha\beta}(\xi_1,\xi_2,\xi_3)=\sum_{K=1}^{n_{\alpha\beta}}\tilde{\varphi}^I_{\alpha\beta}(\xi_1,\xi_2,\xi_3)E_{\alpha\beta}(\xi^I_1,\xi^I_2,\xi^I_3), \tag{11}$$

where $\tilde{\varphi}^I_{\alpha\beta}$ is the Lagrange polynomial associated to the tying point I, such that $\tilde{\varphi}^I_{\alpha\beta}(\xi^J_1,\xi^J_2,\xi^J_2)=\delta_{IJ}$ at any tying point J associated to the covariant strain $E_{\alpha\beta}$.

Algorithmically, the use of MITCn elements amounts to replace the matrix $\boldsymbol{A}_{\alpha\beta}$, equation (9), by

$$\tilde{\boldsymbol{A}}_{\alpha\beta}(\xi_1,\xi_2,\xi_3)=\sum_{I=1}^{n_{\alpha\beta}}\tilde{\varphi}^I_{\alpha\beta}(\xi_1,\xi_2,\xi_3)\boldsymbol{A}_{\alpha\beta}(\xi^I_1,\xi^I_2,\xi^I_3), \tag{12}$$

in the definition of $E^{\text{cov}}_{\alpha\beta}$, equation (8).

From now on, "direct" strains will be replaced with "assumed" strains, and the superimposed tilde that identifies the assumed ones will be obviated in order to simplify the notation.

2.3. Constitutive equations in shells

One of the characteristic features of the degenerated-solid shell elements is the use of the constitutive laws for continuum solids. So, for an elastic solid, the constitutive law can be written as a function relating $\boldsymbol{E}$ with its work-conjugate stress, the second Piola-second Piola-Kirchhoff stress tensor $\boldsymbol{S}$, i.e.

$$\boldsymbol{S}=\boldsymbol{S}(\boldsymbol{E}). \tag{13}$$

Further, the "basic shell" model assumes that the stress in the direction normal to the midsurface (that of $\boldsymbol{G}^3$) is zero [19]. Then, it is convenient to

refer the constitutive law to a Cartesian frame $\{\boldsymbol{e}_1, \boldsymbol{e}_2, \boldsymbol{e}_3\}$ attached to each point $\boldsymbol{X} \in \mathcal{B}^0$, such that a Cartesian plane, say $\{\boldsymbol{e}_1, \boldsymbol{e}_2\}$, be always tangent to the shell, or more precisely, to the surface $\xi_3 = constant$. At this point, we need to refer $\boldsymbol{E}$ to this Cartesian frame:

$$\boldsymbol{E} = \underbrace{\theta_i^\alpha \theta_j^\beta E_{\alpha\beta}}_{E_{ij}} \boldsymbol{e}_i \otimes \boldsymbol{e}_j, \tag{14}$$

with

$$\theta_i^\alpha = \boldsymbol{G}^\alpha \cdot \boldsymbol{e}_i. \tag{15}$$

Using Voigt notation, the local-Cartesian and the covariant components of $\boldsymbol{E}$ are related by

$$\check{\boldsymbol{E}} = \boldsymbol{\Theta} \check{\boldsymbol{E}}^{\text{cov}}, \tag{16}$$

with

$$\check{\boldsymbol{E}} = \begin{bmatrix} E_{11} & E_{22} & E_{33} & 2E_{12} & 2E_{23} & 2E_{13} \end{bmatrix}^T, \tag{17}$$

$$\check{\boldsymbol{E}}^{\text{cov}} = \begin{bmatrix} E_{11}^{\text{cov}} & E_{22}^{\text{cov}} & E_{33}^{\text{cov}} & 2E_{12}^{\text{cov}} & 2E_{23}^{\text{cov}} & 2E_{13}^{\text{cov}} \end{bmatrix}^T, \tag{18}$$

$$\boldsymbol{\Theta} = \begin{bmatrix} \theta_1^1\theta_1^1 & \theta_1^2\theta_1^2 & \theta_1^3\theta_1^3 & \theta_1^1\theta_1^2 & \theta_1^2\theta_1^3 & \theta_1^3\theta_1^1 \\ \theta_2^1\theta_2^1 & \theta_2^2\theta_2^2 & \theta_2^3\theta_2^3 & \theta_2^1\theta_2^2 & \theta_2^2\theta_2^3 & \theta_2^3\theta_2^1 \\ \theta_3^1\theta_3^1 & \theta_3^2\theta_3^2 & \theta_3^2\theta_3^2 & \theta_1^1\theta_3^2 & \theta_3^2\theta_3^3 & \theta_3^3\theta_1^1 \\ 2\theta_1^1\theta_2^1 & 2\theta_1^2\theta_2^2 & 2\theta_1^3\theta_2^3 & \theta_1^2\theta_2^1 + \theta_1^1\theta_2^2 & \theta_1^3\theta_2^2 + \theta_1^2\theta_2^3 & \theta_1^3\theta_2^1 + \theta_1^1\theta_2^3 \\ 2\theta_2^1\theta_3^1 & 2\theta_2^2\theta_3^2 & 2\theta_2^3\theta_3^3 & \theta_2^2\theta_3^1 + \theta_2^1\theta_3^2 & \theta_2^3\theta_3^2 + \theta_2^2\theta_3^3 & \theta_2^3\theta_3^1 + \theta_2^1\theta_3^3 \\ 2\theta_1^1\theta_3^1 & 2\theta_1^2\theta_3^2 & 2\theta_1^3\theta_3^3 & \theta_1^2\theta_3^1 + \theta_1^1\theta_3^2 & \theta_1^3\theta_3^2 + \theta_1^2\theta_3^3 & \theta_1^3\theta_3^1 + \theta_1^1\theta_3^3 \end{bmatrix}. \tag{19}$$

2.4. The Principle of Virtual Works in degenerated-solid shells

When a shell-like body is modeled using the degenerated-solid-shell FEM, the equilibrium of the body is governed by the Principle of Virtual Works

(PVW) given in the standard form for 3D Solids. Using Lagrangian formulation for large deformation problems and the Green-Lagrange strain $\boldsymbol{E}$ as measure of deformation, the PVW for general solids takes the form:

$$\int_{\mathcal{B}^0} \boldsymbol{S} : \delta\boldsymbol{E}\, \mathrm{d}V = \mathcal{W}^{\mathrm{ext}}(\delta\boldsymbol{u}), \tag{20}$$

for all kinematically admissible displacement variation $\delta\boldsymbol{u}$, $\delta\boldsymbol{E}$ is the Green-Lagrange strain induced by $\delta\boldsymbol{u}$, $\boldsymbol{S}$ is the second Piola-Kirchhoff stress tensor (work-conjugate to $\boldsymbol{E}$), and $\mathcal{W}^{\mathrm{ext}}$ is the work of the external forces (surface tractions and body forces) on the whole body under a displacement $\delta\boldsymbol{u}$.

In "direct" FEM, where $\boldsymbol{X}$ and $\boldsymbol{x}$ are interpolated according to equations (3) and (4) and $\boldsymbol{X}$ is known, the displacement variation can be written as

$$\delta\boldsymbol{u} = \delta\boldsymbol{x} = \boldsymbol{\Phi}\delta\boldsymbol{q}, \tag{21}$$

with

$$\delta\boldsymbol{q} = \begin{bmatrix} \delta\bar{\boldsymbol{x}}_1 \\ \delta\boldsymbol{t}_1 \\ \vdots \\ \delta\bar{\boldsymbol{x}}_N \\ \delta\boldsymbol{t}_N \end{bmatrix}, \tag{22}$$

where $\delta\bar{\boldsymbol{x}}_i$ and $\delta\boldsymbol{t}_i$ denote admissible variations of $\bar{\boldsymbol{x}}$ and $\boldsymbol{t}$ at node i.

Under a variation $\delta\boldsymbol{q}$, the covariant strain components given by equation (8) suffer the following variation (written in Voigt notation):

$$\delta\check{\boldsymbol{E}}^{\mathrm{cov}} = \boldsymbol{B}(\boldsymbol{q})\delta\boldsymbol{q} \tag{23}$$

with

$$\boldsymbol{B}(\boldsymbol{q}) = \begin{bmatrix} \boldsymbol{q}^T \boldsymbol{A}_{11} \\ \boldsymbol{q}^T \boldsymbol{A}_{22} \\ \boldsymbol{q}^T \boldsymbol{A}_{33} \\ 2\boldsymbol{q}^T \boldsymbol{A}_{12} \\ 2\boldsymbol{q}^T \boldsymbol{A}_{23} \\ 2\boldsymbol{q}^T \boldsymbol{A}_{13} \end{bmatrix}. \tag{24}$$

Then, using equation (16), the variation of the local-Cartesian components of $\boldsymbol{E}$ is

$$\delta \check{\boldsymbol{E}} = \boldsymbol{\Theta} \boldsymbol{B} \delta \boldsymbol{q}, \tag{25}$$

where $\boldsymbol{B} \equiv \boldsymbol{B}(\boldsymbol{q})$.

2.5. External forces and couples

The external virtual work, that produced by the displacement $\delta \boldsymbol{u}$ or, equivalently, the nodal variations $\delta \boldsymbol{q}$, is

$$\mathcal{W}^{\text{ext}} = \boldsymbol{F}^{\text{ext}} \cdot \delta \boldsymbol{q}, \tag{26}$$

introducing $\boldsymbol{F}^{\text{ext}}$ as the vector of external forces and couples lumped at the nodes.

2.6. Elimination of the drilling degree of freedom

Following a common practice in the formulation of MITCn elements, we choose to eliminate the drilling degree of freedom, that associated to the rotation of the shell around the director. But differing from the classical works on MITCn, where an additive scheme is used to update the director,

recourse is made to the multiplicative scheme proposed by Simo et al.[11], which avoids singularities for large rotations and guarantees the inextensibility of the director. Using such scheme, the variation of $\boldsymbol{t}$ at node i is expressed as

$$\delta \boldsymbol{t}_i = \tilde{\boldsymbol{\lambda}}_i \delta \boldsymbol{t}_i^* \qquad \text{(no summation over } i,\text{)} \tag{27}$$

where $\delta \boldsymbol{t}_i^*$ is a vector in the plane $\{\boldsymbol{i}, \boldsymbol{j}\}$ of the fixed global Cartesian frame $\{\boldsymbol{i}, \boldsymbol{j}, \boldsymbol{k}\}$, and $\tilde{\boldsymbol{\lambda}}_i$ is the 2×3-matrix made of the first two rows of the orthogonal matrix $\boldsymbol{\lambda}_i$ from the transformation

$$\boldsymbol{t}_i = \boldsymbol{\lambda}_i \boldsymbol{k}. \tag{28}$$

Equation (27) shows that only two degrees of freedom are needed to update the nodal director, eliminating in such a way the drilling degree-of-freedom, making the current formulation have five degrees of freedom per node. Consequently, $\delta \boldsymbol{q}$ is replaced by

$$\delta \boldsymbol{q} = \underbrace{\begin{bmatrix} \boldsymbol{I}_{3\times3} & \boldsymbol{0}_{3\times2} & \cdots & \boldsymbol{0}_{3\times3} & \boldsymbol{0}_{3\times2} \\ \boldsymbol{0}_{3\times3} & \tilde{\boldsymbol{\lambda}}_1 & \cdots & \boldsymbol{0}_{3\times3} & \boldsymbol{0}_{3\times2} \\ \vdots & \vdots & \ddots & \vdots & \vdots \\ \boldsymbol{0}_{3\times3} & \boldsymbol{0}_{3\times2} & \cdots & \boldsymbol{I}_{3\times3} & \boldsymbol{0}_{3\times2} \\ \boldsymbol{0}_{3\times3} & \boldsymbol{0}_{3\times2} & \cdots & \boldsymbol{0}_{3\times3} & \tilde{\boldsymbol{\lambda}}_N \end{bmatrix}}_{\boldsymbol{\Lambda}} \underbrace{\begin{bmatrix} \delta \bar{\boldsymbol{x}}_1 \\ \delta \boldsymbol{t}_1^* \\ \vdots \\ \delta \bar{\boldsymbol{x}}_N \\ \delta \boldsymbol{t}_N^* \end{bmatrix}}_{\delta \boldsymbol{q}^*}, \tag{29}$$

where $\boldsymbol{0}_{i\times j}$ denotes the $i \times j$-zero matrix.

2.7. Discrete equilibrium equations for degenerated-solid shell FEM

By replacing $\delta \boldsymbol{q}$ by $\delta \boldsymbol{q}^*$, taking into account that $\delta \boldsymbol{q}^*$ is arbitrary, and introducing the strain and stress measures in local Cartesian coordinates,

the PVW gives rise to the discrete, nonlinear system of algebraic equations that governs the equilibrium of degenerated-solid-shell FEM:

$$\boldsymbol{R}^* = \boldsymbol{F}^{\mathrm{int}*} - \boldsymbol{F}^{\mathrm{ext}*} = \boldsymbol{0}, \tag{30}$$

where

$$\boldsymbol{F}^{\mathrm{ext}*} = \boldsymbol{\Lambda}^T \boldsymbol{F}^{\mathrm{ext}}, \tag{31}$$

$$\boldsymbol{F}^{\mathrm{int}*} = \boldsymbol{\Lambda}^T \underbrace{\int_{\mathcal{B}^0} \boldsymbol{B}^T \boldsymbol{\Theta}^T \check{\boldsymbol{S}} \, \mathrm{d}V}_{\boldsymbol{F}^{\mathrm{int}}}, \tag{32}$$

where the vector $\boldsymbol{F}^{\mathrm{int}}$ of nodal internal forces and couples is introduced, with $\check{\boldsymbol{S}}$ denoting the vector made of the components S_{ij} of the stress tensor $\boldsymbol{S}$ with respect to the local-Cartesian frame $\{\boldsymbol{e}_i\}$ ordered according to Voigt notation:

$$\check{\boldsymbol{S}} = \begin{bmatrix} S_{11} & S_{22} & S_{33} & S_{12} & S_{23} & S_{13} \end{bmatrix}^T. \tag{33}$$

3. Inverse finite element analysis

In inverse finite element analysis, the loaded configuration B as well as the external loads responsible of deforming the shell from B^0 to B are assumed to be known. In our previous works [3, 4], we chose to formulate the equilibrium equation over the known configuration B, using Eulerian stress and strain measures. In this work, we adopt a different approach, assuming that both FEM and IFEM have identical governing equation, that given by the discrete equilibrium equation (30), differing only in the fact that knowns and unknowns are interchanged. Let us explicit the functional dependence

on $\boldsymbol{q}$ and $\boldsymbol{Q}$ of the terms involved in the governing equation (30). Considering $\boldsymbol{F}^{\text{int}*}$, we have:

$$\begin{aligned}\boldsymbol{F}^{\text{int}*}(\boldsymbol{Q},\boldsymbol{q}) &= \boldsymbol{\Lambda}^T(\boldsymbol{q}) \int_{\mathcal{B}^0(\boldsymbol{Q})} \boldsymbol{B}^T(\boldsymbol{q})\boldsymbol{\Theta}^T(\boldsymbol{Q})\check{\boldsymbol{S}}(\boldsymbol{Q},\boldsymbol{q})\,\mathrm{d}V(\boldsymbol{Q}) \\ &= \boldsymbol{\Lambda}^T(\boldsymbol{q}) \int_{\mathcal{B}(\boldsymbol{q})} \boldsymbol{B}^T(\boldsymbol{q})\boldsymbol{\Theta}^T(\boldsymbol{Q})\check{\boldsymbol{S}}(\boldsymbol{Q},\boldsymbol{q})\,[J(\boldsymbol{Q},\boldsymbol{q})]^{-1}\,\mathrm{d}v(\boldsymbol{q}), \quad (34)\end{aligned}$$

where the last equality was obtained by a simple change of the integration domain, being J the Jacobian determinant of the transformation from $\mathcal{B}^0$ to $\mathcal{B}$, given by

$$J = \frac{\mathrm{d}v}{\mathrm{d}V} = \frac{(\boldsymbol{g}_1 \times \boldsymbol{g}_2)\cdot \boldsymbol{g}_3}{(\boldsymbol{G}_1 \times \boldsymbol{G}_2)\cdot \boldsymbol{G}_3}. \quad (35)$$

In FEM, $\boldsymbol{F}^{\text{int}*}$ depends on the unknown $\boldsymbol{q}$ via $\boldsymbol{\Lambda}$, $\boldsymbol{B}$ and $\check{\boldsymbol{S}}$, while in IFEM, it depends on the unknown $\boldsymbol{Q}$ via $\boldsymbol{\Theta}$, J and $\check{\boldsymbol{S}}$.

Concerning the external loads, they generally depend on both deformed and undeformed configurations:

$$\boldsymbol{F}^{\text{ext}*}(\boldsymbol{Q},\boldsymbol{q}) = \boldsymbol{\Lambda}^T(\boldsymbol{q})\boldsymbol{F}^{\text{ext}}(\boldsymbol{Q},\boldsymbol{q}). \quad (36)$$

In case of pressure load, that is a configuration-dependent load, $\boldsymbol{F}^{\text{ext}*}$ is constant for IFEM. On the contrary, for a dead load, $\boldsymbol{F}^{\text{ext}*}$ is a nonlinear function of $\boldsymbol{Q}$.

3.1. Solution of the nonlinear equilibrium equation in IFEM

Let us rewrite the equilibrium equations (30) as

$$\boldsymbol{R}^*(\boldsymbol{Q}) = \boldsymbol{F}^{\text{int}*}(\boldsymbol{Q},\boldsymbol{q}) - \boldsymbol{F}^{\text{ext}*}(\boldsymbol{Q},\boldsymbol{q}). \quad (37)$$

When specifically applied to IFEM, the system of equations (37) have $\boldsymbol{q}$ as known and $\boldsymbol{Q}$ as unknown. This is a nonlinear system that will be solved

using the Newton-Raphson scheme: once $\boldsymbol{Q}^{(k)}$ (that is $\boldsymbol{Q}$ at iteration k) is known, $\boldsymbol{Q}$ is updated by solving the following linear equation for $\Delta\boldsymbol{Q}^*$:

$$\boldsymbol{R}^*(\boldsymbol{Q}^{(k+1)}) = \boldsymbol{R}^*(\boldsymbol{Q}^{(k)}) + \boldsymbol{K}^*(\boldsymbol{Q}^{(k)})\Delta\boldsymbol{Q}^* = \boldsymbol{0}, \tag{38}$$

where $\boldsymbol{K}^*$ is the tangent stiffness matrix

$$\boldsymbol{K}^* = \frac{\partial \boldsymbol{R}}{\partial \boldsymbol{Q}^*}, \tag{39}$$

and

$$\Delta\boldsymbol{Q}^* = \begin{bmatrix} \Delta\bar{\boldsymbol{X}}_1 \\ \Delta\boldsymbol{T}_1^* \\ \vdots \\ \Delta\bar{\boldsymbol{X}}_N \\ \Delta\boldsymbol{T}_N^* \end{bmatrix} \tag{40}$$

After solving the linear system (38), the position of the node i at the undeformed midsurface is straightforwardly updated:

$$\bar{\boldsymbol{X}}_i^{(k+1)} = \bar{\boldsymbol{X}}_i^{(k)} + \Delta\bar{\boldsymbol{X}}_i. \tag{41}$$

3.1.1. Update of the material director vector

The iterative update of the nodal material director $\boldsymbol{T}_i$ requires a special treatment due to two reasons: first, to preserve its unit length, and secondly, to transform the 2D-solution $\Delta\boldsymbol{T}_i^*$. We proceed here in a way identical to that proposed by Simo et al. [10] for "direct" shell FEM.

Given the initial guess $\boldsymbol{T}_i^{(0)}$, we compute the rotation matrix

$$\boldsymbol{\chi}_i^{(0)} = (\boldsymbol{k}\cdot\boldsymbol{T}_i^{(0)})\boldsymbol{I}_{3\times 3} + \widehat{\boldsymbol{k}\times\boldsymbol{T}_i^{(0)}} + \frac{(\boldsymbol{k}\times\boldsymbol{T}_i^{(0)})\otimes(\boldsymbol{k}\times\boldsymbol{T}_i^{(0)})}{1+\boldsymbol{k}\cdot\boldsymbol{T}_i^{(0)}}, \tag{42}$$

where $\widehat{\boldsymbol{v}}$ is the skew-symmetric matrix whose axial vector is $\boldsymbol{v}$. Usually, $\boldsymbol{T}_i^{(0)} \equiv \boldsymbol{t}_i$ is adopted as initial guess. In this case, $\boldsymbol{\chi}_i^{(0)} \equiv \boldsymbol{\lambda}_i$ is the orthogonal matrix of equation (28).

Then, once the director $\boldsymbol{T}^{(k)}$ and the rotation matrix $\boldsymbol{\chi}_i^{(k)}$ are known for an iteration k, $\boldsymbol{T}_i$ and $\boldsymbol{\chi}_i$ are successively updated following the next steps:

1. Update of the director:

$$\boldsymbol{T}_i^{(k+1)} = \cos\|\Delta\boldsymbol{T}_i\|\boldsymbol{T}_i^{(k)} + \frac{\sin\|\Delta\boldsymbol{T}_i\|}{\|\Delta\boldsymbol{T}_i\|}\Delta\boldsymbol{T}_i, \tag{43}$$

   with

$$\Delta\boldsymbol{T}_i = \left[\tilde{\boldsymbol{\chi}}_i^{(k)}\right]^T \Delta\boldsymbol{T}_i^*, \tag{44}$$

   where $\tilde{\boldsymbol{\chi}}_i^{(k)}$ is the 2×3-matrix made of the first two rows of $\boldsymbol{\chi}_i^{(k)}$.

2. Update of the rotation matrix:

$$\boldsymbol{\chi}_i^{(k+1)} = \Delta\boldsymbol{\chi}_i\, \boldsymbol{\chi}_i^{(k)}, \tag{45}$$

   with

$$\Delta\boldsymbol{\chi}_i = \cos\|\Delta\boldsymbol{T}_i\|\boldsymbol{I}_{3\times 3} + \frac{\sin\|\Delta\boldsymbol{T}_i\|}{\|\Delta\boldsymbol{T}_i\|}\widehat{\boldsymbol{T}_i^{(k)} \times \Delta\boldsymbol{T}_i} + \frac{1-\cos\|\Delta\boldsymbol{T}_i\|}{\|\Delta\boldsymbol{T}_i\|^2}(\boldsymbol{T}_i^{(k)} \times \Delta\boldsymbol{T}_i) \otimes (\boldsymbol{T}_i^{(k)} \times \Delta\boldsymbol{T}_i). \tag{46}$$

3.2. Computation of the tangent stiffness matrix

The tangent matrix $\boldsymbol{K}^*$ is made of contributions from the internal and external forces:

$$\boldsymbol{K}^* = \frac{\partial \boldsymbol{F}^{\text{int}*}}{\partial \boldsymbol{Q}^*} + \frac{\partial \boldsymbol{F}^{\text{ext}*}}{\partial \boldsymbol{Q}^*} = \boldsymbol{K}^{\text{int}*} + \boldsymbol{K}^{\text{ext}*}. \tag{47}$$

The term $\boldsymbol{K}^{\mathrm{ext}*}$ appears only if the external loads depend on the initial configuration, like dead loads. In any case, it will not receive further consideration here.

The contribution of the internal forces given by equation (34) can be expressed as

$$\boldsymbol{K}^{\mathrm{int}*} = \boldsymbol{\Lambda}^T \left(\boldsymbol{K}^{\mathrm{mat}} + \boldsymbol{K}^{\mathrm{geo}} \right) \frac{\mathrm{d}\boldsymbol{Q}}{\mathrm{d}\boldsymbol{Q}^*}, \tag{48}$$

with

$$\boldsymbol{K}^{\mathrm{mat}} = \int_{\mathcal{B}} \boldsymbol{B}^T \boldsymbol{\Theta}^T \check{\boldsymbol{C}} \frac{\partial \check{\boldsymbol{E}}}{\partial \boldsymbol{Q}} J^{-1} \, \mathrm{d}v, \tag{49}$$

$$\boldsymbol{K}^{\mathrm{geo}} = \int_{\mathcal{B}} \boldsymbol{B}^T \left. \frac{\partial (\boldsymbol{\Theta}^T \boldsymbol{v})}{\partial \boldsymbol{Q}} \right|_{\boldsymbol{v}=\check{\boldsymbol{S}}} J^{-1} \, \mathrm{d}v - \int_{\mathcal{B}} \boldsymbol{B}^T \boldsymbol{\Theta}^T \check{\boldsymbol{S}} J^{-2} \frac{\mathrm{d}J}{\mathrm{d}\boldsymbol{Q}} \, \mathrm{d}v. \tag{50}$$

3.2.1. Computation of $\boldsymbol{K}^{\mathrm{mat}}$

Two matrices remain undefined in the equation (49) for $\boldsymbol{K}^{\mathrm{mat}}$. The first one is

$$\check{\boldsymbol{C}} = \frac{\partial \check{\boldsymbol{S}}}{\partial \check{\boldsymbol{E}}}, \tag{51}$$

which is the matrix (in Voigt notation) containing the tangent moduli $C_{ijkl} = \partial S_{ij} / \partial E_{kl}$ referred to the local-Cartesian base $\{\boldsymbol{e}_i\}$, which are given material properties.

The second one is $\partial \check{\boldsymbol{E}} / \partial \boldsymbol{Q}$ that, given $\check{\boldsymbol{E}}$ by equation (16), is defined as:

$$\frac{\partial \check{\boldsymbol{E}}}{\partial \boldsymbol{Q}} = \frac{\partial}{\partial \boldsymbol{Q}} \left(\boldsymbol{\Theta} \check{\boldsymbol{E}}^{\mathrm{cov}} \right) = \left. \frac{\partial (\boldsymbol{\Theta} \boldsymbol{v})}{\partial \boldsymbol{Q}} \right|_{\boldsymbol{v}=\check{\boldsymbol{E}}^{\mathrm{cov}}} + \boldsymbol{\Theta} \frac{\mathrm{d}\check{\boldsymbol{E}}^{\mathrm{cov}}}{\mathrm{d}\boldsymbol{Q}}. \tag{52}$$

The first term in the r.h.s. of equation (52) is the matrix whose ij-component is

$$\left[\frac{\partial (\boldsymbol{\Theta} \boldsymbol{v})}{\partial \boldsymbol{Q}} \right]_{ij} = \frac{\partial \Theta_{ik}}{\partial Q_j} v_k. \tag{53}$$

Then, it remains to compute $\partial\Theta_{ik}/\partial Q_j$. Given $\boldsymbol{\Theta}$ by equation (19), its derivative with respect to Q_j is completely determined by the knowledge of

$$\frac{\mathrm{d}\theta_i^\alpha}{\mathrm{d}Q_j} = \boldsymbol{e}_i \cdot \frac{\mathrm{d}\boldsymbol{G}^\alpha}{\mathrm{d}Q_j}. \tag{54}$$

Since $\boldsymbol{G}^\alpha \cdot \boldsymbol{G}_\beta = \delta^\alpha_\beta$, we have

$$\frac{\partial G_i^\alpha}{\partial Q_j} = -G_k^\alpha \frac{\partial G_{\beta_k}}{\partial Q_j} G_i^\beta, \tag{55}$$

where it remains to determine $\partial G_{\beta_k}/\partial Q_j$. Taking into account that $\boldsymbol{G}_\beta = (\partial\boldsymbol{\Phi}/\partial\xi_\beta)\boldsymbol{Q}$ when $\boldsymbol{X}$ is interpolated according to equation (3), $\partial G_{\beta_k}/\partial Q_j$ is the kj-component of the matrix

$$\frac{\partial \boldsymbol{G}_\beta}{\partial \boldsymbol{Q}} = \frac{\partial \boldsymbol{\Phi}}{\partial \xi_\beta}. \tag{56}$$

Regarding the second term in the r.h.s. of equation (52), it remains to compute the matrix $\partial\boldsymbol{E}^{\mathrm{cov}}/\partial\boldsymbol{Q}$. Given the covariant strain components $E^{\mathrm{cov}}_{\alpha\beta}$ by equation (8), we have

$$\frac{\partial \check{\boldsymbol{E}}^{\mathrm{cov}}}{\partial \boldsymbol{Q}} = -\boldsymbol{B}^0, \tag{57}$$

being $\boldsymbol{B}^0 \equiv \boldsymbol{B}(\boldsymbol{Q})$ defined by equation (24).

Finally, $\boldsymbol{K}^{\mathrm{mat}}$ takes the form:

$$\boldsymbol{K}^{\mathrm{mat}} = \int_{\mathcal{B}} \boldsymbol{B}^T \boldsymbol{\Theta}^T \check{\boldsymbol{C}} \left.\frac{\partial(\boldsymbol{\Theta}\boldsymbol{v})}{\partial \boldsymbol{Q}}\right|_{\check{\boldsymbol{E}}^{\mathrm{cov}}} J^{-1}\,\mathrm{d}v - \int_{\mathcal{B}} \boldsymbol{B}^T \boldsymbol{\Theta}^T \check{\boldsymbol{C}} \boldsymbol{\Theta} \boldsymbol{B}^0 J^{-1}\,\mathrm{d}v. \tag{58}$$

3.2.2. Computation of $\boldsymbol{K}^{\mathrm{geo}}$

Regarding the first term of $\boldsymbol{K}^{\mathrm{geo}}$, equation (50), it only remains to determine

$$\left[\frac{\partial(\boldsymbol{\Theta}^T\boldsymbol{v})}{\partial \boldsymbol{Q}}\right]_{ij} = \frac{\partial \Theta_{ki}}{\partial Q_j} v_k, \tag{59}$$

where $\partial\Theta_{ki}/\partial Q_j$ can be expressed in terms of $\partial\theta_i^\alpha/\partial Q_j$, equation (54).

Regarding the second term of equation (50), we need to compute $\partial J/\partial Q_j$. Invoking equation (35), we have

$$\frac{\partial J}{\partial Q_j} = -\frac{J}{(\boldsymbol{G}_1 \times \boldsymbol{G}_2)\cdot \boldsymbol{G}_3}\times \\ \varepsilon_{pqr}\left(\frac{\partial G_{1_q}}{\partial Q_j}G_{2_r}G_{3_p} + G_{1_q}\frac{\partial G_{2_r}}{\partial Q_j}G_{3_p} + G_{1_q}G_{2_r}\frac{\partial G_{3_p}}{\partial Q_j}\right), \quad (60)$$

where ϵ_{pqr} is the Levi-Civita or permutation symbol, and $\partial G_{\alpha_i}/\partial Q_j$ is defined by equation (56).

3.2.3. Computation of $\partial\boldsymbol{Q}/\partial\boldsymbol{Q}^*$

Once $\boldsymbol{K}^{\text{mat}}$ and $\boldsymbol{K}^{\text{geo}}$ are completely determined, the complete determination of the tangent stiffness matrix $\boldsymbol{K}^{\text{int}*}$, equation (48), requires to compute

$$\frac{\partial \boldsymbol{Q}}{\partial \boldsymbol{Q}^*} = \begin{bmatrix} \boldsymbol{I}_{3\times3} & \boldsymbol{0}_{3\times2} & \cdots & \boldsymbol{0}_{3\times3} & \boldsymbol{0}_{3\times2} \\ \boldsymbol{0}_{3\times3} & \partial\boldsymbol{T}_1/\partial\Delta\boldsymbol{T}_1^* & \cdots & \boldsymbol{0}_{3\times3} & \boldsymbol{0}_{3\times2} \\ \vdots & \vdots & \ddots & \vdots & \vdots \\ \boldsymbol{0}_{3\times3} & \boldsymbol{0}_{3\times2} & \cdots & \boldsymbol{I}_{3\times3} & \boldsymbol{0}_{3\times2} \\ \boldsymbol{0}_{3\times3} & \boldsymbol{0}_{3\times2} & \cdots & \boldsymbol{0}_{3\times3} & \partial\boldsymbol{T}_N/\partial\Delta\boldsymbol{T}_N^* \end{bmatrix} \quad (61)$$

where we need to determine $\partial\boldsymbol{T}_i/\partial\Delta\boldsymbol{T}_i^*$ by taking into account the update procedure described in Section 3.1.1. By differentiating the updated $\boldsymbol{T}_i$ given by equation (43) with respect to the nodal increment $\Delta\boldsymbol{T}_i^*$, we obtain

$$\frac{\partial \boldsymbol{T}_i^{(k+1)}}{\partial \Delta\boldsymbol{T}_i^*} = \frac{\partial \boldsymbol{T}_i^{(k+1)}}{\partial \Delta\boldsymbol{T}_i}\frac{\partial \Delta\boldsymbol{T}_i}{\partial \Delta\boldsymbol{T}_i^*} = \Bigg[-\frac{\cos\|\Delta\boldsymbol{T}_i\|}{\|\Delta\boldsymbol{T}_i\|}\boldsymbol{T}_i^{(k)}\otimes\Delta\boldsymbol{T}_i + \\ \left(\frac{\cos\|\Delta\boldsymbol{T}_i\|}{\|\Delta\boldsymbol{T}_i\|^2} - \frac{\sin\|\Delta\boldsymbol{T}_i\|}{\|\Delta\boldsymbol{T}_i\|^3}\right)\Delta\boldsymbol{T}_i\otimes\Delta\boldsymbol{T}_i + \\ \frac{\sin\|\Delta\boldsymbol{T}_i\|}{\|\Delta\boldsymbol{T}_i\|}\boldsymbol{I}_{3\times3}\Bigg]\left[\tilde{\boldsymbol{\chi}}_i^{(k)}\right]^T. \quad (62)$$

4. Applications

4.1. Slit annular plate under a lifting line force

Let us consider a given slit annular plate, clamped at one end and deformed by a lifting line force applied at the other end, as shown in Figure 2. The plate has an inner radius $r = 6$ m, an outer radius $R = 10$ m and a thickness $h = 0.03$ m, and lies in the xy-plane. The lifting load $\boldsymbol{q}$ has a magnitude $q = 0.8$ N/m and points normal to the surface of the undeformed plate (i.e., in the direction of the z-axis). The plate is discretized using 10×80 MITC4 finite elements. The plate is made of a Saint Venant-Kirchhoff (linear-elastic) material, with Young modulus $E = 21$ MPa and Poisson ratio $\nu = 0$.

This problem is a popular benchmark for (direct) FEM applied to largely-deformed shells (see [17] and references therein). The solution obtained using MITC4 elements is shown in Figure 2, and it is in very good agreement with the benchmark of Sze et al. [17], who used the reduced-integration elements known as S4R from the commercial code ABAQUS.

Then, the solution for the deformed configuration $\mathcal{B}$ obtained using FEM with MITC4 is adopted as domain of analysis for IFEM (using MITC4 too). In order to validate IFEM, the given undeformed annular slit plate must be recovered as IFEM solution. The accuracy of IFEM to perform this task is measured in terms of:

$$\text{error}(\boldsymbol{X}) = \|\boldsymbol{X}^{\text{FEM}} - \boldsymbol{X}^{\text{IFEM}}\|, \tag{63}$$

$$\text{error}(\boldsymbol{T}) = \|\boldsymbol{T}^{\text{FEM}} - \boldsymbol{T}^{\text{IFEM}}\|, \tag{64}$$

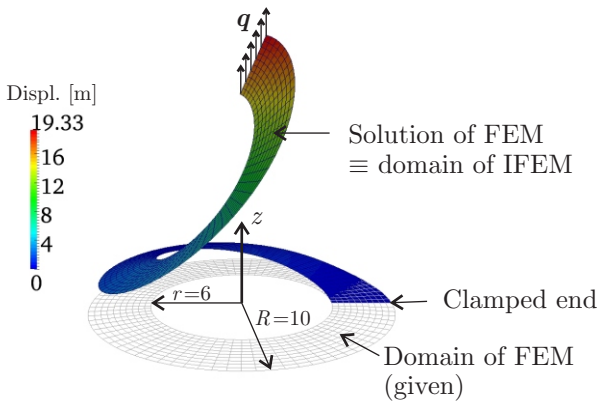

Figure 2: Slit annular plate under large elastic deformation.

where $(*)^{\mathrm{FEM}}$ refers to the nodal variable $(*)$ in the given undeformed configuration (i.e., the domain of analysis of FEM) and $(*)^{\mathrm{IFEM}}$ refers to the nodal variable $(*)$ in the undeformed configuration computed as solution of IFEM. Let us note that $\boldsymbol{T}^{\mathrm{FEM}}$ is the unit vector along the z-axis.

Figure 3 shows how highly accurate is IFEM: maximal error($\boldsymbol{X}$) is 9.3×10^{-6} m (i.e., 7-order-of-magnitude smaller than the maximal displacement magnitude) and maximal error($\boldsymbol{T}$) is 8.5×10^{-7} (being $\boldsymbol{T}$ a unit vector). Let us remark that the FEM problem of obtaining the deformed configuration as well as the IFEM problem of recovering the undeformed configuration were solved using $\|\boldsymbol{R}^*\| < 10^{-6}$ N as convergence criterion for the solution of the nonlinear equilibrium equation (37).

Another remarkable quality of IFEM, already observed in several applications developed in our previous works [3, 4, 6], is the fast convergence to the solution of the nonlinear equilibrium equation (37). When Sze et al. [17] solved the (direct) FEM problem (the one whose solution is the domain of analysis for the current IFEM problem), they reported to need 347 iterations

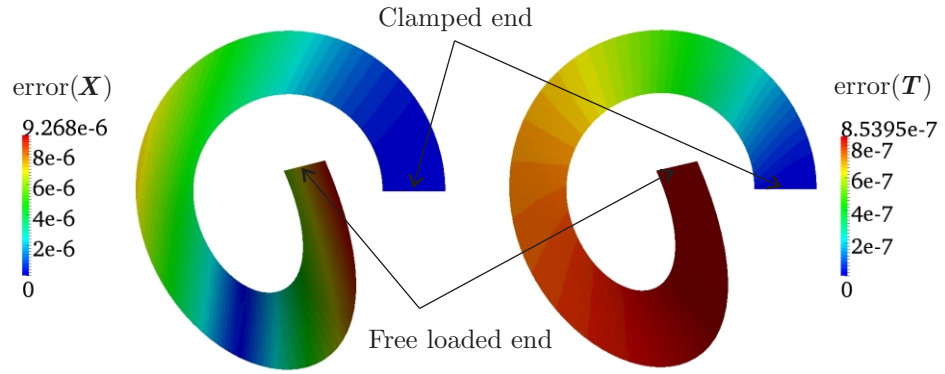

Figure 3: Error of IFEM for recovering the original slit annular plate.

along 67 load increments for the Newton-Raphson solution of the nonlinear equilibrium equation up to a rather large tolerance (0.5% for force and 1% for displacement). On the other hand, the IFEM problem for recovering the original undeformed configuration having the previously FEM-computed deformed configuration as input required only 15 iterations along 2 load steps to solve the nonlinear equilibrium upto the same tolerance.

4.2. Design of a passive microvalve

Now, let us apply IFEM for a real-life inverse design problem: the design of a passive microvalve whose task is identical to that of the microvalve proposed by Seidemann et al. [18], depicted in Figure 4. Integrated to a microchannel with thickness 360 μm and width 200 μm, the valve must close the channel when the pressure drop attains a prescribed value Δp, and bypass a specified flow when the pressure drop vanishes.

Note that the valve in Figure 4, as originally designed by Seidemann et al. [18], cannot remain centered during deformation because its flexible spring is non-symmetric with respect to the direction of the resultant of

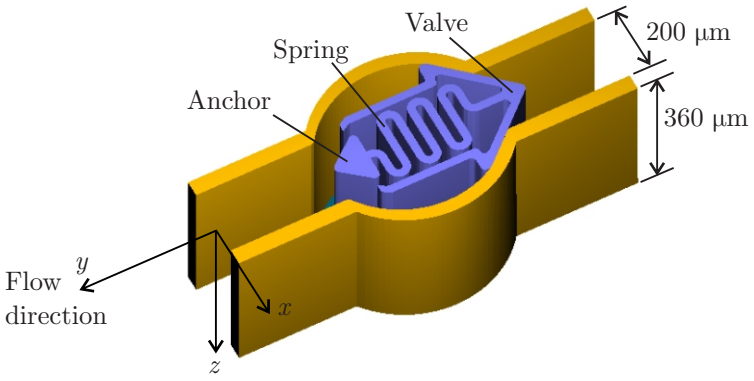

Figure 4: Compliant passive valve to seal a microchannel proposed by Seidemann et al. [18].

the applied pressure. Without information about the pressure drop and the sealing gap, it is not possible to assess how critical is this defect in the design of Seidemann et al. [18]. However, Albanesi et al. [6] directly avoided such defect by replacing the unique non-symmetric spring of the original valve by two springs arranged symmetrically with respect to the axis, as shown in Figure 5b. This symmetric mechanism, where the springs are compliant beams, is the starting point for the current proposal, shown in Figure 5b, where the springs behave as shells.

The valve itself is considerably stiffer than the springs, so it is modeled as a rigid body. Further, given the symmetry of the problem, only one spring is modeled using a mesh of 32850 I-MITC4 shell elements, each one having sides of approximately 2 μm. A detail of this fine mesh is shown in Figure 5c.

The pressure drop Δp determining the closure of the valve was not specified by Seidemann et al. [18]. Let us assume $\Delta p = 1\,\text{kPa}$, which defines the current microvalve as a low-pressure one [21]. The resultant of Δp is a force

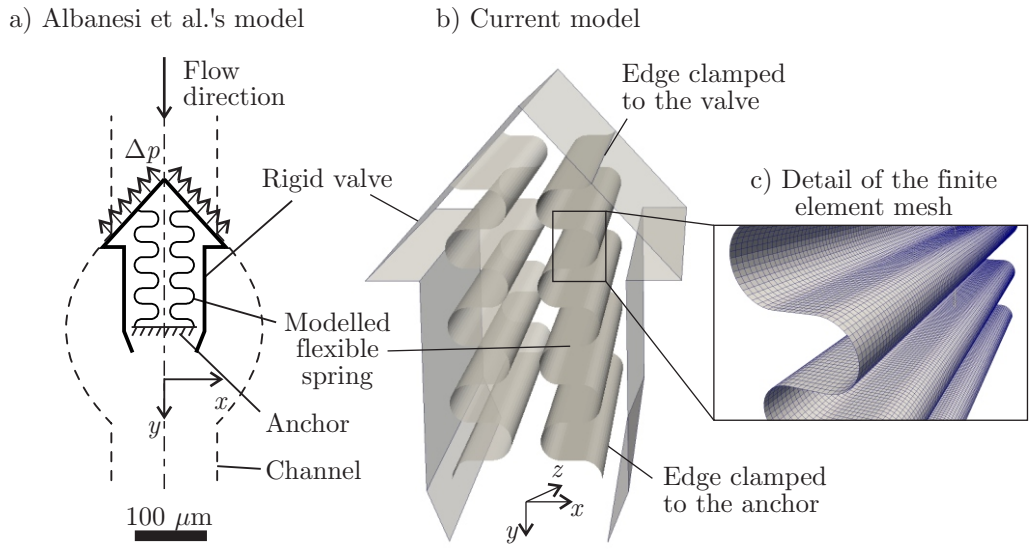

Figure 5: Configuration of a compliant passive valve when closed under a given pressure drop Δp: a) Albanesi et al.'s model [6], where the springs are made of compliant beams; b) current proposal, where the springs are shells; c) detail of the current finite element mesh.

$P = 360\,\mu$ actuating along the axis of the channel (y-axis in Figure 5).

Like those of Seidemann et al. [18] and Albanesi et al.[6], the current valve is made of the monomer SU8, which is assumed to be a linear-elastic material with Young modulus $E = 3.2\,\text{GPa}$ [22], shear modulus $G = 1.2\,\text{GPa}$ [22] and yield strength from 60 to 73 MPa [23].

There is an additional design requirement that can not be *a priori* imposed to IFEM since it involves the valve in its open (i.e., undeformed) condition: a certain sealing gap is needed, depending on the prescribed flow to by-pass. In order to control such gap for given geometry of the deformed midsurface, load and displacement boundary conditions, the thickness of the spring has to be varied. In this case, in order to attain a gap similar to

that of the valve of Albanesi et al. [6], the thickness of the spring is set to $h = 2\,\mu$m, constant.

The Newton-Raphson solution of the nonlinear equilibrium equation required only one load step and four iterations to attain the convergence criterion $\|\boldsymbol{R}^*(\boldsymbol{Q}^{(4)})\| < 10^{-5}\|\boldsymbol{R}^*(\boldsymbol{Q}^{(0)})\|$, being $\boldsymbol{Q}^{(0)}$ the initial guess with components $\bar{\boldsymbol{X}}_i^{(0)} = \bar{\boldsymbol{x}}_i$, $\boldsymbol{T}_i^{(0)} = \boldsymbol{t}_i$, where $\bar{\boldsymbol{x}}_i$ and $\boldsymbol{t}_i$ are the nodal position and director at the node i of the mesh of the given deformed midsurface.

Figure 6a shows the undeformed configuration computed by IFEM. Note that the maximal displacement takes place at the side where the spring is clamped to the valve, so this is the displacement of the rigid valve itself. The magnitude of such displacement is 24.4% of the total height of the spring, which largely justifies the use of the nonlinear theory of large displacements.

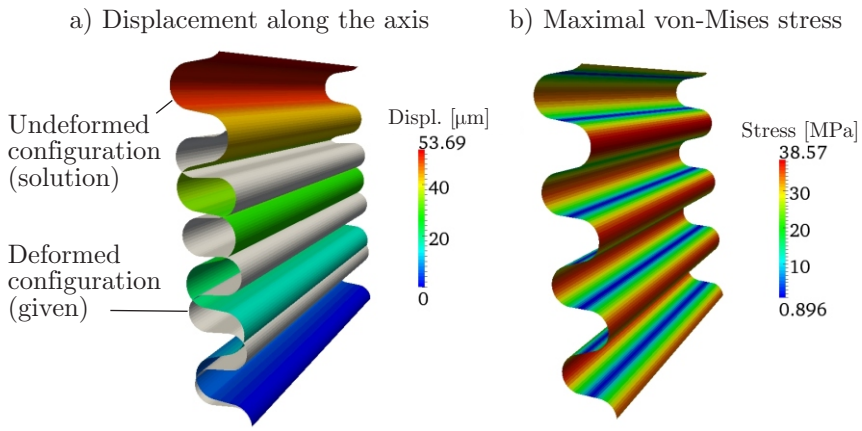

Figure 6: IFEM solution for the compliant passive valve: a) displacement of the midsurface in the direction of the axis of the channel; b) maximal von-Mises stress across the thickness the shell.

In order to assess that the undeformed configuration in Figure 6a actually constitutes the manufacturing shape of the valve, the feasibility of the IFEM

solution has to be evaluated in terms of topological and mechanical tests, as detailed by Albanesi et al. [6]. Concerning topology, IFEM may lead to an useless solution containing inter-penetrated elements. As it can be seen in Figure 6, the current solution is free of such defects.

On the other hand, the mechanical tests concern:

1. *Validity of the hypothesis of elasticity*: assuming the von-Mises yield criterion to hold, this is confirmed by Figure 6b that shows that the maximal von-Mises stress developed throughout the spring, all across its thickness, is considerably lower than the yield strength of SU8 (higher than 60 MPa [23]).
2. *Uniqueness of the solution*, which is lost when an unstable equilibrium state (or critical point) is met during deformation. In the current case, critical points are not passed through the deformation, which is evident for an experienced designer and can be formally confirmed by using the spectrum test [24].

Having succeeded at all these tests, the IFEM-computed undeformed configuration shown in Figure 6 represents in fact the manufacturing shape of the springs of the valve, such that this valve exactly closes the channel under the given pressure drop.

5. Conclusions

This work introduces the inverse finite element method (IFEM) for degenerated-solid shells. IFEM is particularly well suited for the inverse design of compliant mechanisms (in this case, shell-like mechanisms) whose task is to attain a desired shape after large elastic deformations. As a good example

of application of IFEM, the design of a passive valve was undertaken in this work. Such design could also be achieved using an optimization technique, where a FEM problem is solved at each iteration. Here, it was achieved by solving only one IFEM problem.

Further, at the light of the current applications, we observe once again (see our previous works on 3D solids [3] and beams [4, 5, 6]) that the solution of the nonlinear equilibrium equation when the undeformed configuration is unknown (the case of IFEM) takes considerably fewer iterations than the solution of the same equation when the deformed configuration is unknown (the case of FEM).

Last but not least, since degenerated-solid-shell FEM -unlike stress-resultant-shell FEM- makes use of the governing equations from Solid Mechanics, it is easier to reuse the standard material libraries, those where the elastic constitutive laws are written as stress-strain relationships.

Acknowledgments

The research for this paper was financially supported by the European Research Council under the European Union's Seventh Framework Programme (FP/2007-2013) / ERC Grant Agreement N. 320815 (ERC Advanced Grant Project "Advanced tools for computational design of engineering materials COMP-DES-MAT"), and the National Scientific and Technical Research Council of Argentina (CONICET) under the grant PIP 2012-2014 GI-1105.

A. E. Albanesi also thanks the National Technological University of Argentina (UTN) for the grant PID ENUTNFE0002146.

6. References

[1] S. Govindjee and P. A. Mihalic. Computational methods for inverse finite elastostatics. *Comput. Methods Appl. Mech. Engrg.*, 136:47–57, 1996.

[2] S. Govindjee and P. A. Mihalic. Computational methods for inverse deformations in quasi-incompressible finite elasticity. *Int. J. Numer. Meth. Engng.*, 43:821–838, 1998.

[3] V. Fachinotti, A. Cardona, and Ph. Jetteur. Finite element modelling of inverse design problems in large deformations anisotropic hyperelasticity. *Int. J. Numer. Meth. Engng.*, 74:894–910, 2008.

[4] A. E. Albanesi, V. D. Fachinotti, and A. Cardona. Inverse finite element method for large-displacement beams. *Int. J. Numer. Meth. Engng.*, 84: 1166–1182, 2010.

[5] A. E. Albanesi. *Inverse design methods for compliant mechanisms*. PhD thesis, Faculty of Engineering and Water Sciences, National Littoral University, Santa Fe, Argentina, 2011.

[6] A. E. Albanesi, M. A. Pucheta, and V. D. Fachinotti. A new method to design compliant mechanisms based on the inverse beam finite element model. *Mech. Mach. Theory*, 65:14–28, 2013.

[7] J. Lu, X. Zhou, and M. L. Raghavan. Computational method of inverse elastostatics for anisotropic hyperelastic solids. *Int. J. Numer. Meth. Engng.*, 69:1239–1261, 2007.

[8] X. Zhou and J. Lu. Inverse formulation for geometrically exact stress resultant shells. *Int. J. Numer. Meth. Engng.*, 74:1278–1302, 2008.

[9] C.-C. Lan and Y.-J. Cheng. Distributed shape optimization of compliant mechanisms using intrinsic functions. In *Proceedings of the ASME 2007 International Design Engineering Technical Conferences & Computer and Engineering Conference*, Las Vegas, Nevada, USA, September 2007.

[10] J. C. Simo, D. D. Fox, and M. S. Rifai. On a stress resultant geometrically exact shell model. Part III: Computational aspects of the nonlinear-theory. *Comput. Methods Appl. Mech. Engrg.*, 79:21–90, 1990.

[11] J. C. Simo and D. D. Fox. On a stress resultant geometrically exact shell model. Part I: Formulation and optimal parametrization. *Comput. Methods Appl. Mech. Engrg.*, 72:267–304, 1989.

[12] S. Ahmad, B. M. Irons, and O. C. Zienkiewicz. Analysis of thick and thin shell structures by curved finite elements. *Int. J. Numer. Meth. Engng.*, 2:419–451, 1970.

[13] E. Ramm. A plate/shell element for large deflections and rotations. In K.-J. Bathe, J. T.Oden, and W. Wunderlich, editors, *Formulations and Computational Algorithms in Finite Element Analysis: U.S.-Germany Symposium*, pages 264–293. Massachusetts Institute of Technology, 1976.

[14] K.-J. Bathe. *Finite Element Procedures.* Prentice-Hall, Inc., 1996.

[15] E. N. Dvorkin and K.-J. Bathe. A continuum mechanics based four-node shell element for general nonlinear analysis. *Eng. Comput.*, 1: 77–88, 1984.

[16] M. L. Bucalem and K.-J. Bathe. Higher-order MITC general shell elements. *Int. J. Numer. Meth. Engng.*, 36:3729–3754, 1993.

[17] K. Y. Sze, X. H. Liu, and S. H. Lo. Popular benchmark problems for geometric nonlinear analysis of shells. *Finite Elements in Analysis and Design*, 40:1551–1569, 2004.

[18] V. Seidemann, S. Bütefisch, and S. Büttgenbach. Fabrication and investigation of in-plane compliant SU8 structures for MEMS and their application to micro valves and micro grippers. *Sensors and Actuators A*, 97–98:457–461, 2002.

[19] M. L. Bucalem and K.-J. Bathe. *The Mechanics of Solids and Structures. Hierarchical Modeling and the Finite Element Solution.* Computational Fluid and Solid Mechanics. Springer-Verlag, 2011.

[20] D. Chapelle and K.-J. Bathe. *The Finite Element Analysis of Shells. Fundamentals.* Computational Fluid and Solid Mechanics. Springer-Verlag, second edition, 2011.

[21] A. Pandolfi and M. Ortiz. Improved design of low-pressure fluidic microvalves. *J. Micromech. Microeng.*, 17:1487–1493, 2007.

[22] JAHM Sofware, Inc. Material Property Database MPDB v7.41, 2012.

[23] MicroChem Corp. SU-8 permanent photoresists. Table of properties, 2012.

[24] E. L. Allgower and K. Georg. *Introduction to numerical continuation methods.* Society for Industrial and Applied Mathematics (SIAM), 2003.